Memoirs of the Faculty of Science, Kyoto University, Series of Physics, Astrophysics, Geophysics and Chemistry, Vol. XXXV, No. 2 and 3, Article 1, 1979

POLARIZATION IN PROTON-PROTON SCATTERING AT 52 AND 68 MeV

BY

Norio TAMURA

Department of Physics, Faculty of Science, Kyoto University, Kyoto

(*Received October 8, 1977*)

ABSTRACT

The polarization in proton-proton scattering at 52.34 and 68.19 MeV have been measured at 12 angles between 30° and 100° (C.M.) with an accuracy of 0.1~0.3%. The phase shift analysis was performed using the present data. The obtained $^3P_0$-phase shift at 52.34 MeV was 12.99°, which is rather consistent with that by Virginia group but larger than that by Livermore group. The present results were compared with the predictions from theoretical models. The HC–81 potential well fit the experimental data below 150 MeV including the present results.

1. Introduction

It has been known that the main feature of the nucleon-nucleon interaction in the low energy region is due to the exchange of mesons. In the original one-boson exchange contribution (OBEC) model, it is assumed that the dynamical behaviour of the reactions is determined from the matrix elements corresponding to the one-particle exchange. In this model, there is an unrealistic point where an isoscalar scalar meson of several hundred MeV is inevitable, which has been explained as a substitute of two-pion exchange in the same quantum state. Moreover, it was difficult to explain the mean P-wave phase shift at very low energies ($\lesssim$10 MeV) and the $^3P_0$-phase shift between 20 and 200 MeV simultaneously in the simple OBEC model.[1] Some people attempted to resolve these difficulties by substitution of the two-pion exchange contribution for the scalar meson and ρ-meson. But, the definite discussion cannot be made because of the experimental situation.

The P-wave phase shifts can be determined more accurately than other higher waves below 200 MeV because they are dominant except the S-wave which is thought to be out of the applicable region. The ^3P_J-phase shifts show the typical tensor type splitting owing to the one-pion exchange below 20 MeV. But the splitting changes gradually at higher energies because the effects of other mesons in the intermediate region become remarkable. This effect can be seen clearly in the behaviour of $^3P_0$-phase shift in the energy region from 20 to 150 MeV. So, the information in this energy region is very important to study the interaction mechanism at an intermediate region (Region II). In the higher energy region, however, the P-wave may be gradually affected by the innermost and more complicated region.

A considerable amount of data concerning proton-proton scattering are accumulated in this energy region. Those are data on polarization, triple scattering parameters and spin correlation parameters in addition to accurate differential cross section data. But, it has been pointed out that there is inconsistency between A_{XX}

data. Furthermore, the $^3P_0$-phase shifts obtained in phase shift analyses strongly depend on the used data base. For example, the A- and the R-data prefer small values for the $^3P_0$-phase shift though the A_{XX} and C_{NN} data prefer large values. Results of analyses show large scattering of the phase shift from 10° to 15° in the $^3P_0$-state. So, accurate experiments which can determine this phase shift was long waited. It was expected that the measurements on the angular dependence with enough accuracies are effective to eliminate the ambiguity of phase shifts by our preliminary calculation. Though there are some polarization data, they are not so accurate. Moreover, many of those are data at only one angular point. A good polarized proton beam has made it possible to get the data with high accuracy and high statistics at many angles and energies.

2. Experimental details

Schematic view of the experimental set up is shown in Fig. 1.

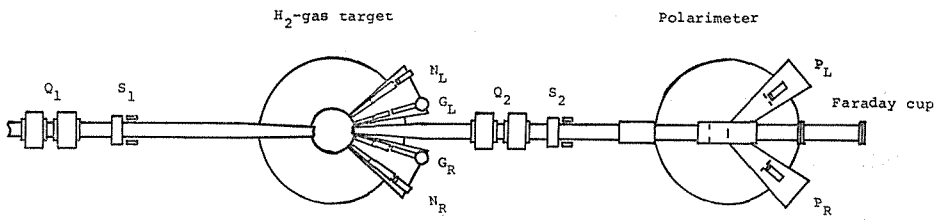

Fig. 1. Schematic view of experimental set up. N's and P's are NaI(Tl) detectors and G's are intrinsic germanium detectors. Q's and S's are quadrupole focusing and steering magnets, respectively.

2.1. Polarized proton beam

The polarized proton beam was produced in a polarized ion source of an atomic beam type. The atomic beam which passed through a sextupole magnet and a radio frequency transition system was ionized in a strong field ionizer of Glavish type. The polarized proton beam was injected axially to the AVF cyclotron at the Research Center of Nuclear Physics, Osaka University. The beam intensity at the target was about 15 nA at 52 MeV and 30 nA at 68 MeV. The beam polarization was higher than 70%. The sign of the beam polarization was flipped by reversing the current of a solenoid of the ionizer. This reversing action was triggered by a signal from a current integrator. The period was 10~15 sec. So, the false asymmetry due to long time drifts was largely reduced.

The possible change of the scattering angle associated with change of the sign of beam polarization was checked by the forward scattering from Au target. As the differential cross section of p–Au scattering has a very steep angular dependence at forward angles (15°~17°), the relative yields are very sensitive to the angle. No appreciable change of the beam direction depending on the sign of beam polarization was seen. The change of the angle was estimated to be smaller than 0.01°. Moreover, the Faraday cup was split into two parts to monitor the position of the beam through the experiment. The change of the beam position was not observed.

The polarization of proton-proton scattering at 45° in the center of mass system has a strong energy dependence. The dependence can be expressed as

$$p = a \cdot E^b,$$

where p is the p–p polarization in percent unit, $\log_{10} a = \bar{6}.64 \pm 1.84$ and $b = 3.36 \pm 1.73$.[2] So, the energy calibration error of 1% corresponds to Δp of 0.1% at 50 MeV. At the higher energy, this is more severe. The energy calibration of the proton beam was performed to reduce this error. The beam was scattered by polyethylene target at the angle of 25°. The scattered particles was detected by two plastic scintillation counters to measure the flight time between those counters. The energy was calibrated with an accuracy of 0.2%. This result was consistent with a calculated value from the analyzing magnet field. Details are described in Appendix A.

2.2. Gas target

A chamber of 240 mm diameter was filled with hydrogen gas. It had stainless steel foils of 4 μm thick on the entrance and exit ports to isolate the gas from vacuum. It had also wide windows of 50 μm thick Mylar foils on the sides for the scattered particles. The chamber was connected to a gas supply system with an electric manometer. The experiment was done at a pressure of about 2 atm. The hydrogen gas was high purity gas of commercial grade.

2.3. Detecting system

Four detector systems were used. On each side of the beam, two detector systems were placed on a turntable. One for smaller angles was an intrinsic germanium detector and the other for larger angles was a NaI(Tl) scintillation detector. In front of these detectors, there were double slit systems to define the target region and the scattering angle. The maximum angular acceptance of the slit was $\pm 1°$. The left and the right detectors were arranged symmetrically to the beam. The setting error was estimated to be smaller than 0.02°. The angular scale was calibrated by the scattering from methane gas. The angular dependence of the energy of scattered protons was measured in the vicinity of the angle where the energy of scattered protons off proton was equal to that off carbon inelastically scattered. The energy was calibrated precisely as described before, the measured cross over angles and the calculated one could be compared. There was no difference larger than 0.05°. In proton-proton scattering, the differential cross section and the polarization at the laboratory angles larger than 15° are smooth and slowly varying function of angles. So, this accuracy is enough in the present experiment.

2.4. Polarimeter

The beam polarization was continuously monitored by a pair of NaI(Tl) scintillation detectors at the down stream of the scattering chamber. A polyethylene film of 30 μm$\sim$60 μm thickness was used as the target. The detectors were set symmetrically to the beam at the angle for the maximum analyzing power.

The calibration of the polarimeter was performed in a separate experimental term. The calibration is described in Appendix B.

2.5. Electronics

A block diagram of the electronics is shown in Fig. 2. Signals of all detectors were analyzed by multichannel pulse height analyzers after passing through self-gated linear gates. The signal from a single channel discriminator was also fed to a scaler

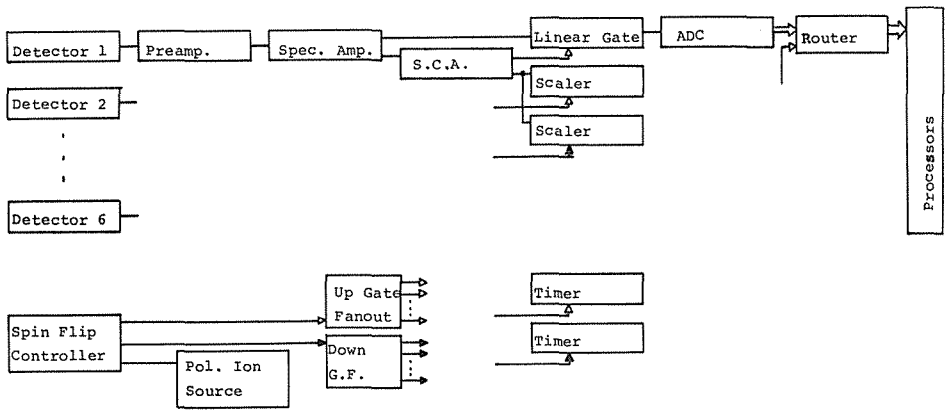

Fig. 2. A block diagram of the electronics used in the present experiment.

whose counting loss was negligible. The counting losses of multichannel analyzers could be corrected with this system. A signal was fed from a spin flip controller of the polarized ion source as a gate signal of 'up' or 'down' state. Scalers were gated by this signal. A specific bit of output data bits from the analog-to-digital converter (ADC) was replaced by this level signal to offset the data. By this routing circuit, the data of the two spin states were converted by one ADC and stored in different memory locations. The stored data were dumped into magnetic tapes and paper tapes.

3. Data reduction and results

A typical spectrum of forward detectors is shown in Fig. 3. Subtraction of the background was as follows. The both sides of the p–p peak were cut off. The cut off channels were determined so that the yields at the channels were nearly equal to those of the background which were, in many cases, 10^{-2} times of the peak as shown by the dashed lines in the figure. This procedure was safely applied because the asymmetry of the background at low energy side was equal to that of the p–p peak. As a check, the subtraction was done as shown by the dash-dotted line in the figure. The results did not change appreciably. Furthermore, the higher cut off level of about 10^{-1} of the peak was also tried as shown by the dotted lines. The results did not change, either. These three procedures of the subtraction of background were performed for all runs. Unnegligible changes were seen in a few runs, exceptionally. These runs were those for forward angles and the contamination were rather large. Elastic peaks from contamination were perfectly separated from the p–p peak. But in those runs, some effects of inelastic scattering was not negligible. The subtraction error was estimated to be about 0.1% and added to the error.

There were four data at one data point. Those were the data of the left and the right detectors for both spin directions. When the yields are defined as L_u, L_d, R_u and R_d, those can be written as follows.

$$L_u = \sigma(\theta_L^u) \cdot N_b^u \cdot N_t^u \cdot \Delta\Omega_L \cdot (1 + P(\theta_L^u) \cdot P_b^u),$$

$$L_d = \sigma(\theta_L^d) \cdot N_b^d \cdot N_t^d \cdot \Delta\Omega_L \cdot (1 - P(\theta_L^d) \cdot P_b^d),$$

$$R_u = \sigma(\theta_R^u) \cdot N_b^u \cdot N_t^u \cdot \Delta\Omega_R \cdot (1 - P(\theta_R^u) \cdot P_b^u)$$

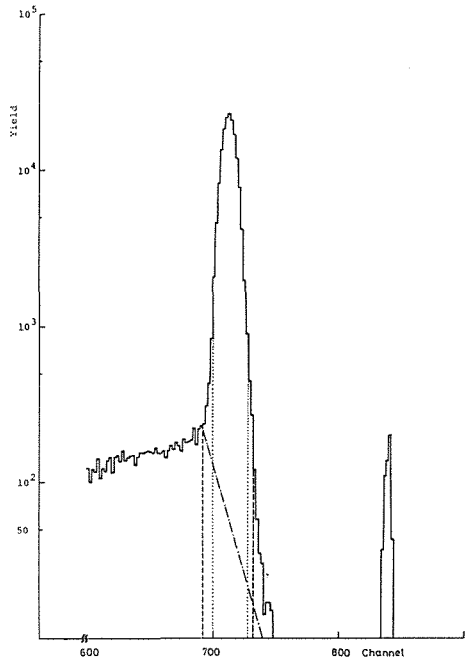

Fig. 3. A typical spectrum and subtractions.

and

$$R_d=\sigma(\theta_R^d)\cdot N_b^d\cdot N_t^d\cdot \Delta\Omega_R(1+P(\theta_R^d)\cdot P_b^d),$$

where $\sigma(\theta)$, N_b, N_t, $\Delta\Omega$, $P(\theta)$ and P_b are the differential cross section, number of protons in the beam, number of protons in the target, solid angle of the detector, polarization of p–p scattering and beam polarization, respectively. The suffixes u and d mean the direction of the beam polarization. As described before, the sign of beam polarization was frequently changed. So, N_t^u could be thought to be equal to N_t^d. If $\theta_L^u=\theta_L^d=\theta_R^u=\theta_R^d=\theta$ and $P_b^u=P_b^d=P_b$, the asymmetry can be gotten as follows.[3]

$$\varepsilon=P_b\cdot P(\theta)=\frac{L-R}{L+R},$$

where $L=\sqrt{L_u\cdot R_d}$ and $R=\sqrt{R_u\cdot L_d}$. The quantities N_b, N_t and $\Delta\Omega$'s cancel each other in this approximation. As described before, the assumption for angles was sufficiently good. If P_b^d is not equal to P_b^d, the asymmetry can be obtained as the product of the p–p polarization and the mean polarization of the beam, approximately. The beam polarization was also monitored by a polarimeter at the same time. The asymmetry was calculated by the same way. So, the mean polarization appears again. The ratio of the two asymmetries (at the first and the second target) is meaningful. Then the effect almost disappears. Even if the difference of the beam polarization is 10%, the resultant polarization is estimated to differ less than 0.02% from true one in the present case. This difference is small enough in comparison with the statistical error of about 0.1~0.3%. The maximum angular acceptance of

$\pm 1°$ is so small that the error on the asymmetry due to the angular variation of polarization and differential cross section can be neglected.

The false asymmetry was checked using a nearly unpolarized beam which was

Table 1. Results of the present experiment. Quated errors are relative errors. Normalization error is estimated as 2%.

	52.34 MeV			68.19 MeV		
θ_L	θ_{CM}	P	ΔP	θ_{CM}	P	ΔP
15.0	30.40	0.0313	0.0017			
15.5				31.54	0.0609	0.0018
18.0	36.47	0.0335	0.0023	36.61	0.0651	0.0028
18.5	37.48	0.0366	0.0025			
20.0				40.66	0.0674	0.0024
22.5	45.56	0.0359	0.0012	45.73	0.0643	0.0029
25.0				50.79	0.0624	0.0030
26.5	53.63	0.0335	0.0017			
30.0				60.89	0.0522	0.0033
30.5	61.70	0.0305	0.0016			
35.0	70.74	0.0232	0.0009			
35.5				71.97	0.0359	0.0017
38.0	76.77	0.0161	0.0019	76.99	0.0246	0.0025
38.5	77.77	0.0153	0.0012			
40.0				81.01	0.0217	0.0021
42.5	85.79	0.0051	0.0011	86.02	0.0089	0.0025
45.0				91.02	−0.0017	0.0025
46.5	93.79	−0.0027	0.0015			
50.0				101.01	−0.0260	0.0028
50.0	101.78	−0.0126	0.0015			

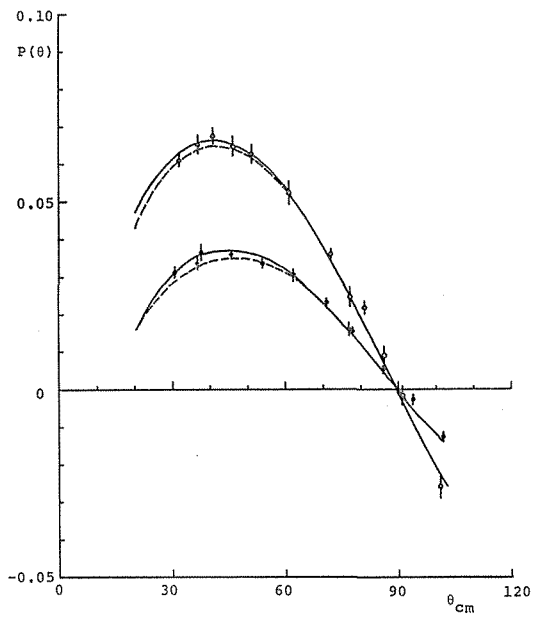

Fig. 4. Results of the present experiment. Close circles and open circles are data at 52.34 and 68.19 MeV, respectively. Solid and broken curves are values calculated by the solution of the present analysis and that of the energy dependent analysis of AHR–II.

produced by cutting off the radio frequency oscillator of the r.f. transition section of the ion source. The result was consistent with an expected value in the experimental accuracy.

The result is shown in Table 1 and Fig. 4. The relative errors which are written in the table are mainly from statistics. The errors at laboratory angles of 15° and 18.5° at 52.34 MeV include those caused by inelastic scattering by contamination.

4. Phase shift analysis

Energy independent phase shift analyses were performed using the present data combined with other existing data.[4] In the analyses, contributions from partial waves higher than the F-waves were given by the OBEC model with K-matrix unitarization. Parameters in the OBEC calculation are given in Table 3.

4.1. 52. 34 MeV

(1) Data base

Many experimental data were accumulated at about this energy. However, some of those are old and not so accurate because of technical restrictions. Therefore, only a part of them were used in the present analyses.

The correction for the energy was necessary for those data except differential cross section and polarization data. In the present analyses, energy dependences of data at different energies were assumed to be equal to those calculated using the phase shifts of the energy dependent analysis by Virginia group (AHR–II).[5] The A_{XX} and D-parameter were almost energy independent but the energy dependence of A- and R-parameter were not negligible. Data used in the present analyses were listed in Table 2.

Table 2. Final data base used in the present analysis. N is a number of the data and M is χ^2 contribution of the data in the six parameters analysis.

	Energy	N	M	Reference
	52.34 MeV			
σ	52.34	29	23.1	J. Sanada et al. ref. 10
P	52.34	12	6.29	Present data
R	47.8	5	8.54	A. Ashmore et al. ref. 16
A	47.8	5	2.41	A. Ashmore et al. ref. 16
C_{NN}	52.34	1	0.04	Interpolated data
A_{XX}	46.9	1	2.45	D. Garreta et al. ref. 19
D	50	1	0.29	T. C. Griffith et al. ref. 20
	68.19 MeV			
σ	68.3	26	38.4	D. E. Young et al. ref. 22
P	68.19	12	8.54	Present data
C_{NN}	68.19	1	0.69	Interpolated data

i) Differential cross section

There are data by U. E. Kruse et al.,[6] by J. N. Palmieri et al.,[7] by K. Nisimura et al.,[8] by J. C. Batty et al.[9] and J. Sanada et al.[10] Data by Palmieri et al., by Kruse et al. and by Nisimura et al. have large errors. Data by Batty et al. seem to be

accurate by the quoted error. But, data by Sanada et al. obtained in a gas target experiment are accurate enough, which are consistent with those by Batty et al. Because of this reason, the present experiment was performed at the same energy as theirs. Quoted relative errors were employed in the analyses, for the normalization factor must be treated as another factor. The normalization factor was not searched because it seemed to be difficult that the normalization factor was determined in the single energy analysis using only one data set for differential cross sections. Though an analysis was done using the normalization factor given by Arndt et al.,[11] no remarkable change was found, especially in the P-states.

ii) Polarization

There had existed polarization data by J. N. Palmieri et al., by[7] P. Christmas et al.[12] and by C. J. Batty et al.[13] before the present experiment was done. Though the datum by Batty et al. is rather accurate, it is only at one angular point and consistent with the present data. So, it will give a small effect when it is combined with the present data. It is necessary to correct the energy difference when it is used in the analysis. For these reasons, the datum was not used. Other data are consistent with the present data but not accurate enough. So, those data were not used in the present analyses.

iii) Other parameters

Data of C_{NN} and C_{KP} by K. Nisimura et al.[14] were not used because those are not so accurate and may be replaced with more accurate data which were obtained by new technique such as a polarized beam and a polarized target. As several C_{NN} data[15] exist below 100 MeV, it is possible to get an interpolated value at 52.34 MeV, it is possible to get an interpolated value at 52.34 MeV. So, the interpolated value was used for this parameter. As R- and A-parameter data, those by A. Ashmore et al. at 47.8 MeV[16] were used. There is another set of A-parameter data at 47.5 MeV by the same group.[17] Because it was published prior to the another set by the same group, it was thought to be better to choose the latter data. So, data at 47.5 MeV were omitted in the final data base. An analysis was also done using the omitted A-data. The result will be discribed later. There are two A_{XX} data; one by K. Nisimura et al.[18] (INS A_{XX}) and another by D. Garreta et al.[19] Those data are seriously inconsistent with each other. The calculated energy dependence of A_{XX} by the result of energy dependent analysis prefered the data by Garreta et al. Moreover, the data by Garreta et al. was obtained by the experiment with a polarized beam. So, it must have less possibilities to include systematic errors. Therefore, the data by Garreta et al. was used for the final data base. But, an analysis was also done using another data. The data of D-parameter by T. C. Griffith et al.[20] was also used in the analyses. But, the data did not contribute so much to the results because it is only one angular point data and not so accurate.

(2) Results and discussion on the analyses

The phase shifts of $^1S_0$-, ^3P_J-, $^1D_2$-waves and ε_2 were freely searched. The phase shifts of $^3F_3$- and $^3F_4$-wave were fixed to values of the energy dependent analysis of AHR–II. A phase shift of the $^3F_2$-wave was fixed as other ^3F_J-phase shifts in one case and it was freely searched in another case, for the phase shift couples with the $^3P_2$-phase shift. The difference of the $^3P_0$-phase shift in the two cases was not so much. Results of the present analyses are shown in Table 3. Results of the six parameters search are shown in Fig. 5 with results of analyses by others. Results of the present analyses were consistent with those of analyses by M. H. MacGregor

et al. (MAW–X)[21] and AHR–II except in the $^3P_0$-state. The $^3P_0$-phase shift of the present analysis is rather consistent with that of AHR–II but contradicts with that of MAW–X. Starting values of phase shifts were values of energy dependent analysis of AHR–II. Different starting values gave no meaning effect to the results.

Analyses on different data bases were done as a check of present analyses. Results of those analyses are shown in Table 4. Scattering of the results are seen in Fig. 6. Although the $^3P_0$-phase shift still scattered wider region than the other

Table 3. Results of the present phase shift analysis. The n_D is degrees of freedom and the C.L. is confidence level which was read from a figure in "Review of particle properties"

	52.34 MeV	52.34 MeV	68.19 MeV	68.19 MeV
$^1S_0$	38.16±0.06	38.29±0.10	33.87±0.62	33.83±0.77
$^3P_0$	12.99±0.16	12.82±0.15	8.41±3.66	8.48±3.51
$^3P_1$	−8.43±0.04	−8.29±0.06	−10.47±0.19	−10.73±0.33
$^3P_2$	5.89±0.06	5.90±0.05	8.41±0.59	8.41±0.51
$^1D_2$	1.62±0.04	1.69±0.04	2.52±0.10	2.27±0.19
ε_2	−1.66±0.04	−1.75±0.05	−2.07±0.15	−1.70±0.17
$^3F_2$	(0.32) fixed	0.17±0.10	(0.44) fixed	0.78±0.18
n_D	48	47	33	32
χ^2	43.14	41.44	47.59	39.86
C.L.	~65%	~75%	~5.5%	~18%

	π	S	ρ	ω
Mass (MeV)	137.5	450.0	750.0	750.0
$G^2/4\pi$	144.4	2.56	21.90	8.29
$Gf/4\pi$			8.42	2.56
$f^2/4\pi$			3.24	0.79

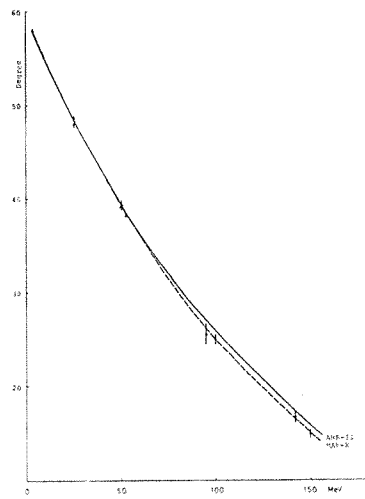

Fig. 5–a. $^1S_0$-phase shift. Solid and broken line are results of energy dependent analysis of AHR–II and MAW–X. Close circles and open circles are results of energy independent analysis of AHR–II and MAW–X. The cross is the result of the present analysis with six parameters.

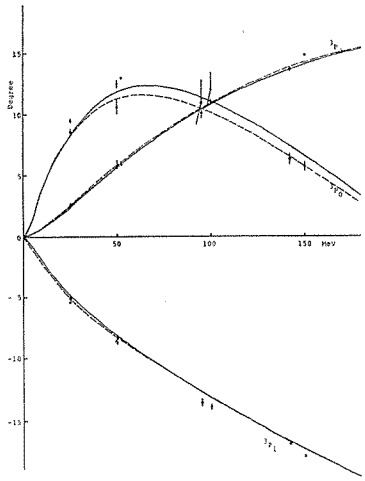

Fig. 5-b. ^3P_J-phase shifts.

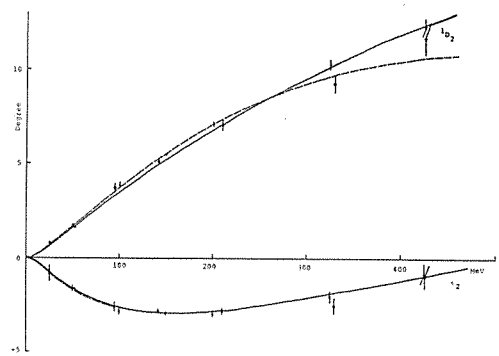

Fig. 5-c. $^1D_2$- and ε_2-phase shift.

Table 4. Analyses in different conditions at 52.34 MeV. N and $\bar{\chi}^2$ are a number of data and a $\bar{\chi}^2$ value divided by degrees of freedom.

	1	2	3	4	5	6	7	9	8
$^1S_0$	38.16 ±0.16	38.21 ±0.22	38.23 ±0.07	38.26 ±0.10	38.14 ±0.08	38.09 ±0.17	38.24 ±0.15	38.11 ±0.15	38.02 ±0.08
$^3P_0$	12.99 ±0.41	13.24 ±0.31	12.94 ±0.20	12.30 ±0.41	13.15 ±0.26	13.54 ±0.62	12.31 ±0.27	13.30 ±0.52	12.99 ±0.10
$^3P_1$	−8.43 ±0.08	−8.39 ±0.12	−8.39 ±0.08	−8.49 ±0.09	−8.43 ±0.04	−8.38 ±0.12	−8.49 ±0.10	−8.40 ±0.04	−8.51 ±0.04
$^3P_2$	5.89 ±0.08	5.82 ±0.10	5.88 ±0.07	6.04 ±0.10	5.86 ±0.07	5.77 ±0.15	6.04 ±0.09	5.83 ±0.11	5.93 ±0.05
$^1D_2$	1.62 ±0.06	1.53 ±0.15	1.63 ±0.02	1.62 ±0.02	1.59 ±0.06	1.59 ±0.08	1.65 ±0.02	1.61 ±0.08	1.67 ±0.02
ε_2	−1.66 ±0.07	−1.57 ±0.16	−1.68 ±0.02	−1.64 ±0.03	−1.64 ±0.06	−1.64 ±0.07	−1.67 ±0.03	−1.67 ±0.08	−1.71 ±0.02
N	54	41	54	53	49	49	54	54	42
$\bar{\chi}^2$	0.90	0.82	0.90	0.82	0.80	0.92	1.11	1.36	1.01

Comments

1 Final data base. Different starting values.
2 Only σ and P.
3 Final data base. (Normalization of P)=0.98.
4 (Final data base)−(A_{xx})
5 (Final data base)−(R)
6 (Final data base)−(A)
7 (Final data base)−(A)+(A(47.5 MeV))
8 (Final data base)−(A_{xx})+(INS A_{xx})
9 (Final data base)−(P)

phase shifts, the $^3P_0$-phase shifts obtained in the present analyses fell in the region of 12.3°∼13.5°. This scattered region is fairly narrower than that of the previous results of 10°∼15°. This smallness of the scattering will give a strong restriction in the study on models. The A- and R-parameter data prefered small values for the

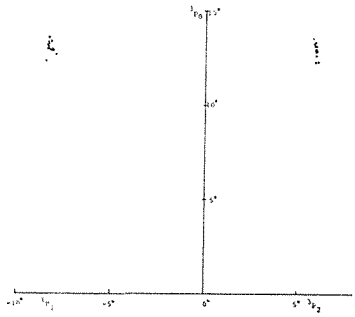

Fig. 6. Scattering of ${}^3P_J$-phase shifts obtained on different data bases.

${}^3P_0$-phase shift, and the A_{XX} data prefered a large value conversely. The INS A_{XX} data gave a large value for the ${}^3P_0$-phase shift even when A- and R-data were included. It also gave a large error on the ${}^3P_0$-phase shift and the χ^2-value. Conversely, the A-data at 47.5 MeV gave the small ${}^3P_0$-phase shift despite of including A_{XX} data, and the error for the phase shift and the χ^2-value were also large. By these facts, it can be said that the omission of those two data were reasonable. Even if the normalization of 0.98 for the present polarization was adopted, the result did not change remarkably. An analysis using only differential cross section and polarization data was also done. The results were consistent with other analyses.

4.2. 68. 19 MeV

There are only data of differential cross section by D. E. Young et al.[22] except unaccurate data of excitation function around this energy. Therefore, the differential cross section data by Young et al., an interpolated C_{NN} data and the present polarization data were used in the analyses. The data base and the result are also shown in

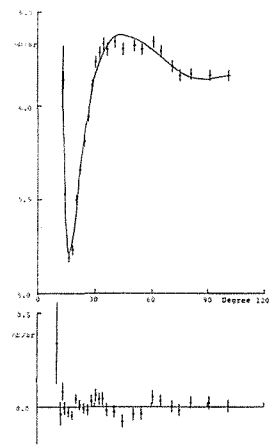

Fig. 7. Data of differential cross section at 68.3 MeV and the calculated value by obtained phase shifts. The lower figure shows differences of the data and the calculated values.

Table 2 and Table 3. From the result, it can be said that the $^3P_1$- and $^3P_2$-phase shift were consistent with other results, but the $^3P_0$-phase shift could not be well determined on this data base. The differential cross section data gave a very large χ^2-value. For this reason, there is a possibility that the differential cross section data have larger relative errors than quoted ones in their paper. This question will be supported by Fig. 7. The analysis in which the C_{NN} data was omitted gave the large $^3P_0$-phase shift of 15.37°. The calculated value of C_{NN} at 90° (C.M.) by this result was 0.266 whereas the interpolated value by the experimental data was 0.147. As seen in Table 5, the results were scattered widely though the scattering was within the errors. So, the present result at 68.19 MeV must not be considered to be confirmed and more data are needed. This comment would be confirmed by extremely small values for confidence levels as shown in Table 3.

Table 5. Analyses in different conditions at 68.19 MeV. Notations are same as in Table 4.

	1	2	3
$^1S_0$	33.76±0.53	32.33±0.00	33.80±0.53
$^3P_0$	9.05±3.15	15.37±3.20	9.64±2.85
$^3P_1$	−10.50±0.10	−10.45±0.19	−10.46±0.11
$^3P_2$	8.32±0.55	7.21±0.61	8.18±0.47
$^1D_2$	2.52±0.07	2.58±0.11	2.51±0.10
ε_2	−2.10±0.13	−2.34±0.12	−2.13±0.12
N	39	38	39
$\bar{\chi}^2$	1.44	1.34	1.42

Comments
1 Final data base. Different starting values.
2 Only σ and P.
3 Final data base. (Normalization of P)=0.98

5. Discussions

The results of the present analysis and others are shown in Fig. 8 together with calculated values by some models. Differences between those models were remarkably seen especially in the $^3P_0$-state.

The Hamada-Johnston potential[23] and Reid's soft core potential[24] gave too small $^3P_0$-phase shifts. Those were consistent with the results of MAW–X at 25 and 50 MeV but not consistent with those of AHR–II and the present result. On the contrary, the HC–81 potential by R. Tamagaki et al.[25] which had smaller core radius and a little stronger tensor and LS potential than Hamada-Johnston potential could fairly well fit the results of AHR–II and the present analysis in all ^3P-states and also in ^3F-states. The mean phase shift $^3\Delta_C$ below 10 MeV calculated by this potential was also consistent with the experimental data as shown in Fig. 9. From these facts, it can be said that the HC–81 potential is a good potential to describe the ^3P-waves and ^3F-waves at least to 150 MeV. But, this model failed to fit the experimental data in the F-states above 300 MeV due to non static effects as already pointed out by the authors themselves.

Recent results of one-boson exchange potential in the momentum space by M. Wada[26] are also shown in Fig. 8. The model could fit fairly well to the ex-

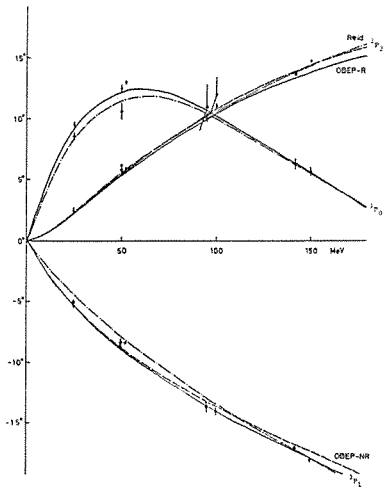

Fig. 8-a

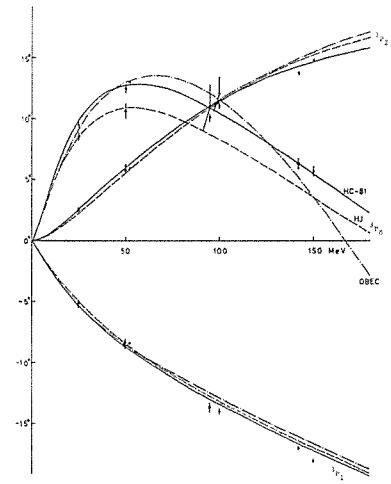

Fig. 8-b

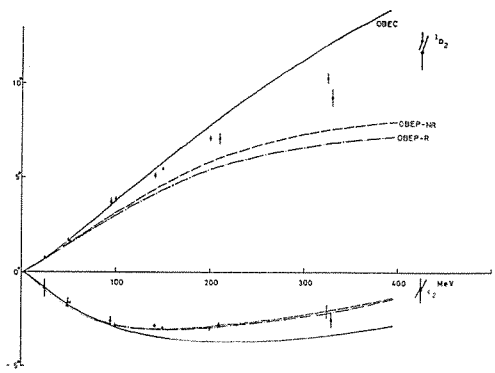

Fig. 8-c

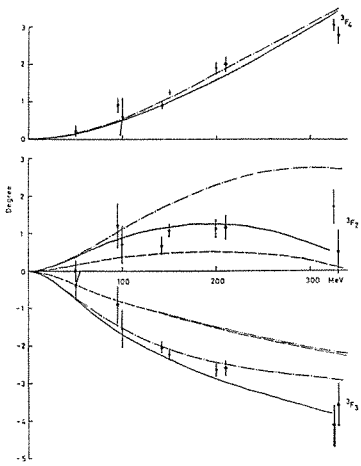

Fig. 8-d

Fig. 8-a. Calculated phase shifts by some models and experimental phase shifts for ^3P_J-state. Experimental data are shown by the same symbols as in Fig. 5. The solid line, the broken line and the dash-dotted line are values calculated by HC–81 potential, Hamada-Johnston potential and the OBEC model.

Fig. 8-b. The solid line, the broken line and the dash-dotted line were calculated by OBEP in momentum space with retardation effects, by OBEP without the effects and Reid's soft core potential.

Fig. 8-c. $^1D^3$- and ε_2-phase shifts. The solid, the broken and the dash-dotted lines were calculated by OBEC, OBEP without retardation effects and OBEP with the effects. The dotted line was calculated by HC–81.

Fig. 8-d. ^3F_J-phase shifts. The solid, the dash-dotted, the broken and the dash-dot-dotted lines are values calculateb dy HC–81 potential, the OBEC model, OBEP without retardation effects and OBEP with the effects.

perimental results in the ^3P-states, too. But, it could not fit so well in the $^1D_2$-state and ^3F-states as the HC–81 potential could do.

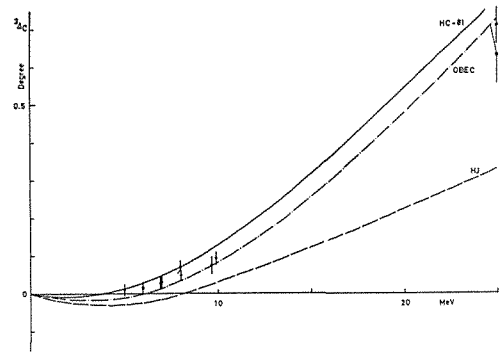

Fig. 9. Mean phase shift of ${}^3P_J$-wave, ${}^3\Delta_C$, below 25 MeV. The solid, the broken and the dash-dotted lines are values calculated by HC–81 potential, Hamada-Johnston potentail and the OBEC model.

It was pointed out that the simple OBEC model could not describe the behaviour of ${}^3P_0$-wave at about 50 MeV and ${}^3\Delta_C$ below 10 MeV. But results of the present analysis and AHR–II which gave large ${}^3P_0$-phase shifts changed the situation. The phase shift calculated by the OBEC model whose parameters were modified to fit the ${}^3P_0$-phase shift are also shown in Fig. 8 and in Fig. 9. As the calculation was not to search a minimum point in χ^2-space, the parameters are not on the best values. Moreover, the parameters do not fit n–p data because the present fitting is only in the p–p state. The OBEC model whose parameters are shown in Table 6 gave rather good fit to the experimental data of the ${}^3P$-waves below 150 MeV. But, calculated values of higher partial waves, such as ${}^1D_2$, ${}^3F_J$ etc., at higher energies did not well fit the experimental data. Especially, the ${}^3F_2$-phase shift was too large.

Table 6. OBEC parameters to fit the experimental data. S denotes the scalar meson.

	π	S	ρ	ω
Mass (MeV)	137.5	420.0	750.0	750.0
$G^2/4\pi$	14.2	2.55	24.0	8.28
$Gf/4\pi$			8.82	2.57
$f^2/4\pi$			3.24	0.80

It will be effective to avoid this difficulty that a lighter scalar meson is added to fit ${}^3\Delta_C$ below 10 MeV. Actually, it would be more realistic that the scalar meson which is not found and the ρ-meson which has a large width are replaced by two pions in the exchange contribution model, which can give effective contributions due to the continuous mass from low mass. More intensive studies on this problem will be done hereafter.

The most distinct difference between the potential models above examined and the OBEC model is the energy dependence of the ${}^3P_0$-phase shift at about 100 MeV. So, it is very useful to determine the phase shifts accurately at least one energy point near 100 MeV to clarify these problems.

ACKNOWLEDGMENTS

The author would like to express his gratitude to Prof. K. Nisimura for his continuous encouragements and guidances through this work. He also wishes to acknowledge Dr. K. Imai for his collaboration and valuable discussions. He is deeply grateful to Prof. Y. Wakuta, Drs. T. Saito, H. Sato, H. Hasuyama, H. Yamamoto, Messrs. K. Egawa, K. Hatanaka, H. Shimizu and Y. Mori for their collaboration in carrying out this experiment.

Thanks are also due to Prof. W. Watari for furnishing the computer code for the phase shift analysis. He also wishes to thank Prof. R. Tamagaki and Dr. M. Wada for their offering numerical values of their calculations. His thanks are also due to Prof. K. Miyake for his critical reading of the manuscript and fruitful discussions. The author's thanks are also due to the staffs of the AVF cyclotron at the Research Center for Nuclear Physics for their helps.

Appendix A

The energy of the beam from AVF cyclotron of Research Center of Nuclear Physics of Osaka University is determined by an analyzing magnet system.[27] Nominal energy value is given by the magnetic field analysis. The magnetic field is continuously monitored by a NMR system.

Polarization of proton-proton scattering has a rather strong energy dependence. To eliminate the error due to the energy determination, the beam energy was calibrated accurately by measuring the flight time of scattered protons. The schematic view of the experimental set up is shown in Fig. 10. Incident protons of 45.14 MeV nominally were scattered by a 60 μm polyethylene target at the center of a scattering chamber to the direction of 25°. The protons passed through a 50 μm Mylar window, a 0.5 mm plastic scintillation counter (S_1) which produced start signals for a time to amplitude converter circuit (TAC), an evacuated duct with two 50 μm Mylar windows and a 3 mm plastic scintillation counter (S_2) which produced stop signals for the TAC. A defining aperture of 3 mm diameter was placed in front of S_1 counter. The duct of 6247 mm length was evacuated to about 0.1 Torr by a rotary pump.

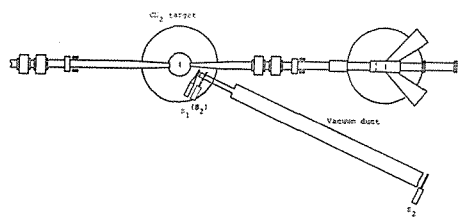

Fig. 10. Schematic view of the experimental set up in the energy calibration run. S_1 and S_2 are trigger counters to measure the flight time of scattered protons. At a first step, the S_2 was placed as shown by a dotted line.

1. Measurements of the flight time

The measurements were performed in two steps. At the first step, S_2 counter

was placed 80 mm behind S_1 counter to compensate the intrinsic delays of both counter systems. Then, as the second step, S_2 counter was placed 6335 mm behind S_1 counter. A time scale of the system was obtained using a time calibrator circuit whose accuracy was 10 psec nominally. A block diagram of the electronics is shown in Fig. 11.

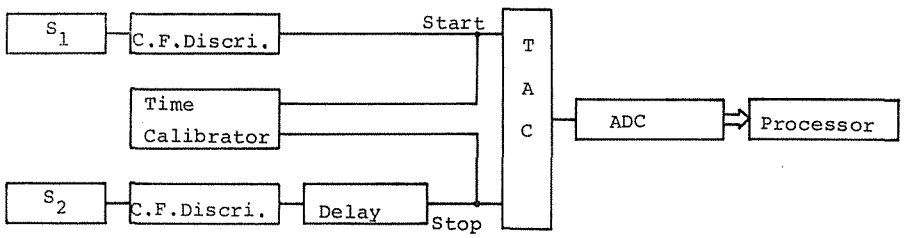

Fig. 11. A block diagram of the electronics in the energy calibration run.

2. Energy losses

There were several sources of energy losses of incident and scattered protons. Some of them were calculated.[28] Energy losses used for correction are shown in Table 7.

Table 7. Energy losses in energy calibration experiment.

Stainless steel foil (4 μm)	0.0292 MeV
CH_2 target (60 μm)	0.0888 MeV
Mylar window (50 μm)	0.0921 MeV
Air (85 mm)	0.1255 MeV
S_1 counter and Mylar foil	0.6325 MeV

1) Entrance foil

The scattering chamber had an entrance foil of 4 μm stainless steel. The energy loss in the foil was calculated on the approximation that the foil was made of iron.

2) Target

The stopping power of polyethylene was calculated by the equation of

$$\frac{dE}{d\rho} = \frac{1}{14}(2x+12z) \qquad \text{MeV } g^{-1}\text{cm}^2,$$

where x (MeV g^{-1} cm^2) and z (MeV g^{-1} cm^2) are stopping power of hydrogen and carbon, respectively.

3) Mylar window of the scattering chamber

The scattered paricles went out through a 50 μm Mylar window of the scattering chamber. The stopping power of Mylar was also calculated by a similar equation as done for polyethylene.

$$\frac{dE}{d\rho} = \frac{1}{192}(8x+64y+120z) \qquad \text{MeV}g^{-1}\text{cm}^2,$$

where the additional parameter y denotes the stopping power of oxygen in the unit of MeV g^{-1} cm^2.

4) Trigger counter (S_1) and a Mylar window of the vacuum duct

The scattered protons from a polyethylene target were detected by an intrinsic germanium detector to obtain the energy scale for the multichannel pulse height analyzer. Then the trigger counter (S_1) and a Mylar film of same thickness as the window were placed between the scattering chamber and the detector to measure the energy loss.

5) Air

The energy loss in the air was also calculated.

3. Result

The beam energy calculated from the measured energy of scattered protons was 45.150 ± 0.072 MeV, where the expected value from the magnetic field analysis was 45.14 MeV. Those values were completely consistent with each other in the experimental accuracy. Estimated errors are listed in Table 8.

Table 8. Errors due to several sources in energy calibration run.

Measurement of distance between S_1 and S_2	0.14 cm	
Measurement of flight time	0.043 ns	
	Sub total	0.061 MeV
Setting	0.1°	0.006 MeV
Energy loss estimation		0.037 MeV
	Total	0.072 MeV

Appendix B

Polyethylene targets were set at the first and second target point. At each target, one pair of detectors were set, respectively. The experimental set up is shown in Fig. 12. In the calibration run, the first system at the upstream was regarded as a polarimeter. The angular dependence of the asymmetry of p–C elastic scattering was measured by the second system. Then, the energy for second system was degraded by a degrader of Al and/or C. In this way, asymmetries for some energy points were measured relatively to the first system. Then the incident energy for the first system was lowered by changing the operating condition of the cyclotron. The same procedure was performed again. Energy and angle of the two sets of measurements were, of course, overlapped. Finally, a helium–4 gas target was set at the first target position to normalyze to the data of p–^{4}He elastic scattering by Berkeley group at 45 MeV.[29] When the measured analyzing power was normalized to the Berkeley data, the maximum analyzing power of p–C scattering obtained in this measurement slightly exceeded 100%. By this reason, the normalization factor was so determined that the maximum polarization was 100%. This procedure corresponds to give a normalization factor of 0.98 to the Berkeley data. Total normalization error was estimated as 2%. Detailes will be described in another paper.

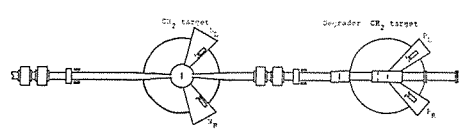

Fig. 12. Schematic view of the set up in the calibration experiment of the polarimeter.

REFERENCES

1) K. Imai, K. Nisimura, H. Sato and N. Tamura; Bull. of Inst. for Chem. Research, Kyoto Univ. **52** (1974) 142.
K. Imai, K. Nisimura, N. Tamura and H. Sato; Nucl. Phys. **A246** (1975) 76.
2) P. Christmas and A. E. Taylor; Nucl. Phys. **41** (1963) 388.
3) G. G. Ohlsen and P. W. Keaton, Jr.; Nucl. Instr. Meth. **109** (1973) 41.
4) These analyses have been performed with the FACOM M190 computer at the Data Processing Center, Kyoto University.
5) R. A. Arndt, R. H. Hackman and L. D. Roper; Phys. Rev. **C15** (1977) 1002.
6) U. E. Kruse, J. M. Teem and N. F. Ramsey; Phys. Rev. **101** (1956) 1079.
7) J. N. Palmieri, A. M. Cormack, N. F. Ramsey and R. Wilson; Ann. Phys. **5** (1958) 299.
8) K. Nisimura, J. Sanada, I. Hayashi, S. Kobayashi, D. C. Worth, H. Imada, N. Ryu, K. Fukunaga, H. Hasai, Sung Baik Nung and Y. Hiradate; INSJ **45** (1961).
9) C. J. Batty, T. C. Griffith, D. C. Imrie, G. J. Lush and L. A. Robbins; Nucl. Phys. **A98** (1967) 489.
10) J. Sanada, K. Kuriyama, Y. Takeuchi, Y. Nojiri, N. Ryu, H. Hasai, M. Ikeda, S. Kobayashi, K. Nagamine, D. C. Worth and T. Yamaya; Nucl. Phys. **B4** (1968) 379.
11) R. A. Arndt, R. H. Hackman and L. D. Roper; Phys. Rev. **C9** (1974) 555.
12) P. Christmas and A. E. Taylor; Nucl. Phys. **41** (1963) 388.
13) C. J. Batty, R. S. Gilmore and G. H. Stafford; Nucl. Phys. **45** (1963) 481, Phys. Lett. **2** (1962) 109.
14) K. Nisimura, J. Sanada, P. Catillon, K. Fukunaga, T. Hasegawa, H. Hasai, N. Ryu, D. C. Worth and H. Imada; Prog. Theor. Phys. **30** (1963) 719.
15) P. Catillon, M. Chapellier and D. Garreta; Nucl. Phys. **B2** (1967) 93.
D. Garreta, K. Nisimura and M. Fruneau; Phys. Lett. **31B** (1970) 363.
D. Garreta and M. Fruneau; Nucl. Phys. **A170** (1971) 492.
K. Nisimura, T. Hasegawa, T. Saito, E. Takasaki, N. Horikawa, T. Nakanishi, M. Saito, S. Sugimoto, T. Yamaki and H. Ueno; Phys. Lett. **30B** (1969) 612.
O. N. Jarvis, T. W. P. Brogden, B. Rose, J. P. Scanlon, J. Orchard-Webb and M. R. Wigan; Nucl. Phys. **A108** (1968) 63.
16) A. Ashmore, B. W. Davies, M. Devine, S. J. Hoey, J. Litt, M. E. Shepherd, R. C. Hanna and L. P. Robertson: Nucl. Phys. **73** (1965) 256.
17) A. Ashmore, M. Devine, B. Hird, J. Litt, W. H. Range, M. E. Shepherd and R. L. Clarke; Nucl. Phys. **65** (1965) 305.
18) K. Nisimura, T. Hasegawa, T. Saito, E. Takasaki, N. Horikawa, T. Nakanishi, M. Saito, S. Sugimoto, T. Yamaki and H. Ueno; Phys. Lett. **30B** (1969) 612.
19) D. Garreta and M. Fruneau; Nucl. Phys. **A170** (1971) 492.
20) T. C. Griffith, D. C. Imrie, G. J. Lush and A. J. Metheringham; Phys. Rev. Lett. **10** (1963) 444.
21) M. H. MacGregor, R. A. Arndt and R. M. Wright; Phys. Rev. **182** (1969) 1714.
22) D. E. Young and L. H. Johnston; Phys. Rev. **119** (1960) 313.
23) Y. Hamada and I. D. Johnston; Nucl. Phys. **34** (1962) 382.
24) R. V. Reid, Jr.; Ann. Phys. **50** (1968) 411.
25) R. Tamagaki and W. Watari; Suppl. Prog. Theor. Phys. **39** (1967) 23.
26) M. Wada; Private communication.
27) RCNP Annual Report 1976.
28) H. Bichsel; Technical Report No. 2 (1961).
J. B. Marion and F. C. Young; Nuclear Reaction Analysis, North-Holland.
29) A. D. Bacher, G. R. Plattner, H. E. Conzett, D. J. Clark, H. Grunder and W. F. Tivol; Phys. Rev. **C5** (1972) 1147.